Bioanalytics

International Edition: DOI: 10.1002/anie.201502615
German Edition: DOI: 10.1002/ange.201502615

Printable Bioelectronics To Investigate Functional Biological Interfaces

*Kyriaki Manoli, Maria Magliulo, Mohammad Yusuf Mulla, Mandeep Singh, Luigia Sabbatini, Gerardo Palazzo, and Luisa Torsi**

Keywords:
capacitance · chiral resolution · organic transistors · sensors · thermodynamics

Dedicated to Professor Pier Giorgio Zambonin on the occasion of his 80th birthday

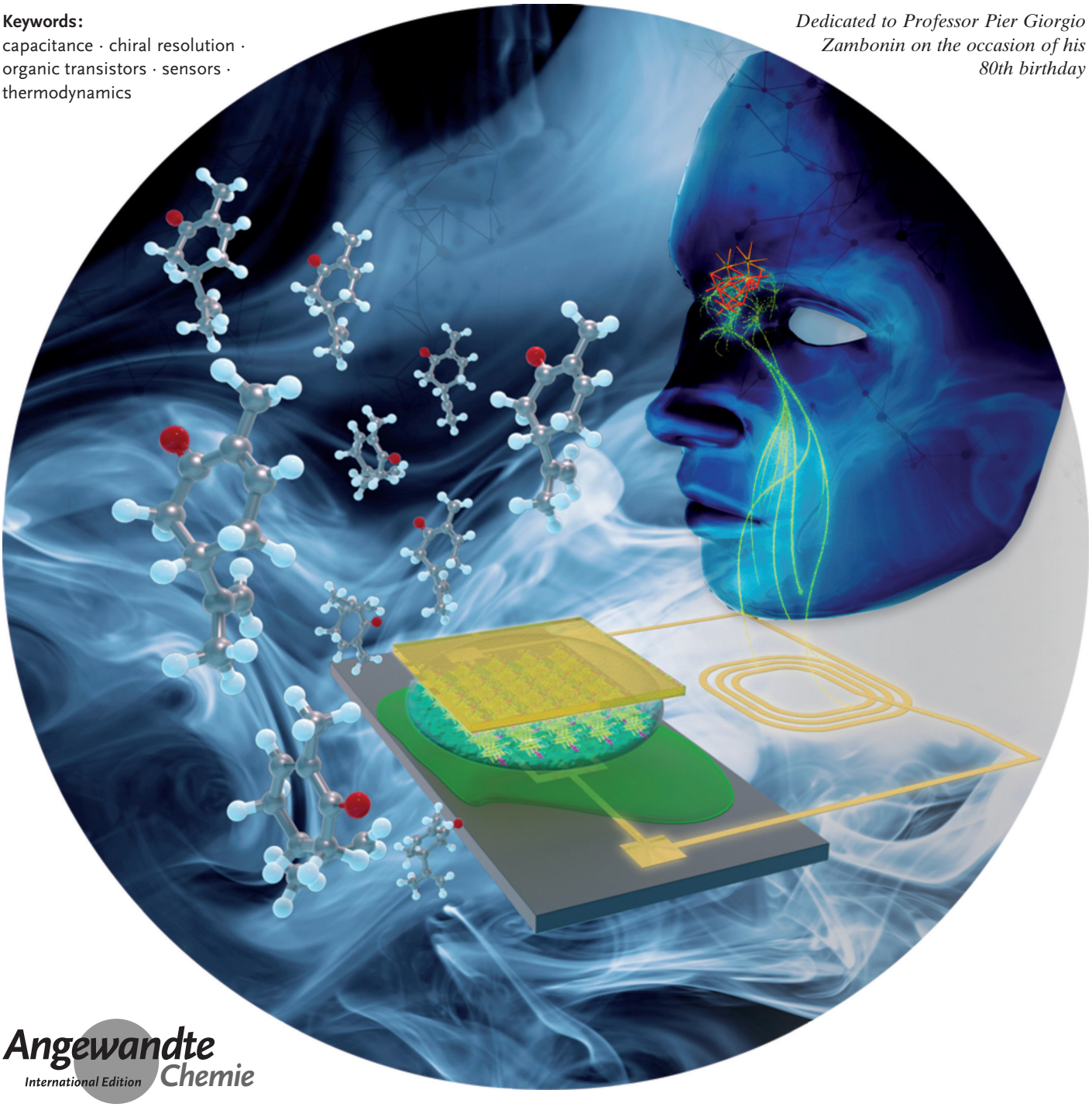

Thin-film transistors can be used as high-performance bioelectronic devices to accomplish tasks such as sensing or controlling the release of biological species as well as transducing the electrical activity of cells or even organs, such as the brain. Organic, graphene, or zinc oxide are used as convenient printable semiconducting layers and can lead to high-performance low-cost bioelectronic sensing devices that are potentially very useful for point-of-care applications. Among others, electrolyte-gated transistors are of interest as they can be operated as capacitance-modulated devices, because of the high capacitance of their charge double layers. Specifically, it is the capacitance of the biolayer, being lowest in a series of capacitors, which controls the output current of the device. Such an occurrence allows for extremely high sensitivity towards very weak interactions. All the aspects governing these processes are reviewed here.

From the Contents

1. Introduction

Bioelectronics is a highly interdisciplinary research field that aims at the development of key technologies to investigate biological interfaces as well as to face novel challenges in life sciences.[1] It currently encompasses the development of applications in the field of biosensing devices[2] and in areas involving the development of novel tools to study neural interfaces.[3] Bioelectronic studies also concern the engineering of new tissues[4] as well as the realization of more-controlled and biocompatible drug-delivery systems.[5]

The study of the mechanisms involved in processes such as those governing the biochemical interactions occurring between a recognition element (R), integrated into an electronic device, and its ligand (L) play an important role in bioelectronics.[6] In this respect, the study of how the binding of L to R changes as the biological species changes from being dispersed in a solution to being confined on a surface is critically important, but very seldom investigated. The acquired knowledge can also be critically important to realize ultrasensitive biological and chemical sensors.[6]

Some of the bioelectronic devices proposed so far are fabricated by printing compatible techniques and such an approach has proven valuable to realize tools for applications such as disposable biosensors[7a,b] or even resorbable devices.[8] The latter class of bioelectronic systems can be implanted and, eventually, do not need to be explanted once they have accomplished their task. As far as the sensors are concerned, the digital quality of the analytical electronic response and the ultralow detection limits foreseen will offer the possibility of performing reliable quantitative assays of proteins (and biomarkers in general) in biological fluids such as saliva or tears. Here, the biomarkers are present at the femtomolar (fM) level or lower. Eventually, a label-free, non-invasive strip test can be conceived that is based on bioelectronic sensors printed at low cost. To this end, organic electronics or, more general, printing biotechnologies could be the privileged choice to fabricate such devices on plastic[9] or even paper substrates.[10] Interestingly, even the biological layer can be deposited by printing.[11] It is, therefore, feasible, although very challenging, to conceive a whole bioelectronic device fabricated by printing. This would result in electronic strips that can be developed, in principle, at costs comparable to those of already commercially available disposable test strips, which are capable of delivering semiquantitative responses at best.

The availability of disposable and low-cost electronic strip tests that are fabricated by printing and are capable of delivering a response whose analytical quality is comparable to that of bench-top facilities for biochemical analysis, holds the potential to revolutionize the current approach to point-of-care testing. Indeed, the global market for such biosensors is estimated to reach over 15 billion dollars by 2020, with approximately 50% share of the point-of-care applications.[12] This is the rationale behind the choice of centering this Review on bioelectronic microdevices based on solution-processed organic semiconductors as well as on printable metal oxides (e.g. ZnO),[13] carbon nanotubes,[14] and graphenes.[15]

Several research groups have contributed to the advancements in the field of printed bioelectronics, proposing novel structures that integrate a layer of biological recognition or functional elements that are directly coupled to one of the electronic interfaces of the thin-film transistor (TFT). The bioelectronic systems proposed so far include organic, electronic ion pumps that allow the delivery of ions and neurotransmitters,[16] biomedical implants,[17] as well as electronic membranes that form intimate contacts with biological tissues to be electronically controlled.[18] These systems are based on organic or printable bioelectronic transistor structures (mostly TFT,[19] but also field-effect transistors, FETs[20]) with diverse device configurations and operating principles.

[*] Dr. K. Manoli, Dr. M. Magliulo, Dr. M. Y. Mulla, M. Sc. M. Singh, Prof. L. Sabbatini, Prof. G. Palazzo, Prof. L. Torsi
Dipartimento di Chimica
Università degli Studi di Bari "Aldo Moro"
Via Orabona 4, 70126 Bari (Italy)
E-mail: luisa.torsi@uniba.it
Homepage: http://www.luisatorsi.info

These structures include electrochemical transistors,[21] the electrolyte-gated TFTs,[7a,22] the organic charge-modulated FETs,[23] as well as structures involving back gates[24] or double gates.[25]

The devices listed above are usually classified into two main categories: transistors that involve an ionic conductor and those that use an insulator as the dielectric medium. Generally speaking, electrochemical and electrolyte-gated transistors rely on a liquid electrolyte as the dielectric, while all the other structures involve a solid insulator. The sensors that involve a solid dielectric and a back-gate configuration have TFT structures. Typically, the source (S) and drain (D) electrodes contact the printable semiconductor (PSC), while the gate (G) electrode is capacitively coupled to the PSC electronic channel, through the solid dielectric. The two bioelectronic back-gate structures integrate the biological recognition elements either on top of the PSC, as in the bilayer transistor[26] sketched in Figure 1 a, or underneath it, as in the functional bio-interlayer (FBI) transistor of Figure 1 b.[27] The interaction of the affinity ligand (L) with the integrated recognition elements (Rs) has been demonstrated to sensitively and selectively impact the characteristics of the transistors. Indeed, these label-free devices are able to reach detection limits down to the pM level and the reproducibility of the devices is characterized by a relative standard deviation (RSD) of a few percent over several hundred repeated determinations.[28] The robustness and the potential for real-life applications of this label-free approach, is also demonstrated by experiments that show that up to 10^4 repeated measurements in sea water can be performed with low RDS.[29] The organic charge-modulated FETs, which share some similarities with the long-known class of ion-sensitive FETs (ISFETs)[30] have recently resulted in a high-performance referenceless transducer of the electrical activity of electrogenic cells.[31] Electrochemical transistors have also attracted particular interest for chemo- and biosensing applications because of the possibility to implement biocompatible and water-stable organic semiconductors such as poly(3,4-ethylenedioxythiophene):poly(styrenesulfonate) (PEDOT:PSS). The operation mechanism of the electrochemical transistors is based on doping the organic semiconductor,[32] and particularly interesting is the recent demonstration that in vivo recording of brain signals can be performed with this class of devices.[33]

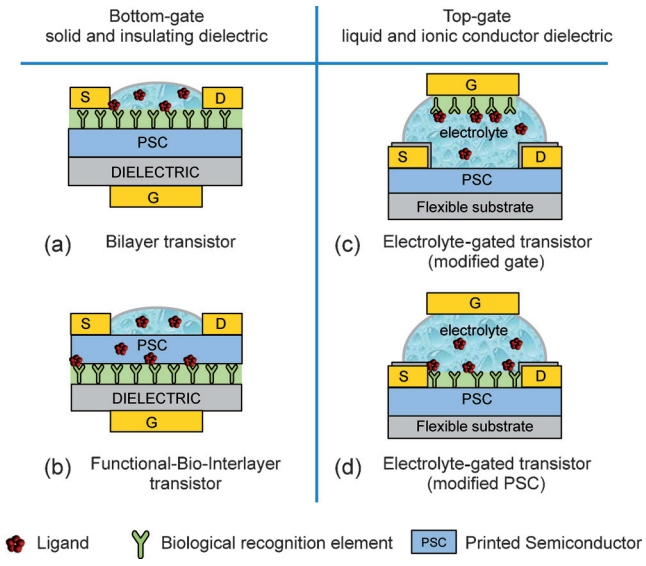

Figure 1. Overview of different bioelectronic device structures involving a bottom or a top gate as well as an insulating or an ionic conducting dielectric.

A number of reviews can already be found on back-gate bilayer[34] and FBI[7,24b] sensors as well as on ISFETs[23a] and electrochemical[22b] transistor sensors, while relatively less discussed are the electrolyte-gated TFTs (EG-TFTs) used for bioelectronic applications.[7a,22a,35] This Review will be mostly restricted to this last class; in particular, the device structures that will be reviewed are those outlined in Figure 1 c,d. Here a top gate is coupled to a PSC through an electrolyte. The structures integrated in the biological recognition layer are either deposited on the gate or on the PSC surface. In both cases, an ionic conductor acts as the dielectric. Besides illustrating the high performance that can be reached in the detection of proteins and small and even neutral molecules, this Review will discuss the high potential of EG-TFTs to investigate a protein interface, particularly when uncharged biological species are involved. Before entering into the details of a bioelectronic EG-TFT structure and function mechanisms, the properties of surface-confined functional biological recognition elements are discussed.

Luisa Torsi completed her degree in physics in 1989 and PhD in chemical sciences in 1993. She was a postdoctoral fellow at Bell Laboratories from 1994 to 1996. In 2010, she was the first female to be awarded the Hedrick Emanuel Merck prize for analytical sciences. She has authored about 150 ISI papers and is co-inventor of several patents. Her principal scientific contributions are in the field of organic bioelectronic devices for sensing applications. Her achievements include the realization of a solid-state device capable of electronic detection of chiral species at ultralow concentrations.

Gerardo Palazzo received a degree in chemistry in 1988 and a PhD in applied chemistry and biochemistry in 2004. He has been coordinator of several research projects at Bari University and CSGI. He is currently Associate Professor in Physical Chemistry and head of BS and MS courses in Chemistry at the University of Bari. He has published more than 100 papers in international peer reviewed journals and books. His main research activities concern the characterization of soft matter by means of physico-chemical techniques, the biophysics of proteins, and the development of novel biosensors.

2. Interface-Confined Biological Recognition Elements

Depending on their nature, biomolecules can perform different biological activities: antibodies, carrier proteins, and nucleic acids can act as molecular recognition elements, molecular motors are able to carry out mechanical work, while enzymes or ribozymes are involved in catalytic reactions. In such processes, the performance level achieved by naturally occurring biomolecules is, as yet, largely unmatched by artificially produced biosystems. In bioelectronic systems the integrated biomolecules are, therefore, preferably produced in living cells or extracted from biological fluids. The biosystems are then deposited on a solid surface, either in their native form or after ad hoc chemical modification, to create a biofunctional interface that can mediate the transduction of biochemical information. The confinement of biological species at surfaces is also important for applications such as those in biocatalysis,[36] bioremediation,[37] and molecular machines.[38] The cases of enzyme-linked immunosorbent assay (ELISA)[39] or of surface-plasmon resonance (SPR)[40] methods can be taken as examples of gold standards in bioassays. Indeed, they rely on biomolecules deposited on solid surfaces such as silica for ELISA and gold for SPR, and show how surface-segregated biological species can retain their biofunctional activity and thus allow for high-throughput and reliable analyses. ELISA assays need a label, while SPR ones need the aid of a label to routinely reach sub-nM detection limits.

From a more fundamental point of view it is interesting to note that the processes associated with biomolecules confined at an interface and occurring at the sub-nanometer length scale can be efficiently revealed by means of a micrometer-sized transducer. For example, the binding of a ligand to a biological recognition element can give rise to effects such as surface displacements, contact angle changes, or electrostatic modifications, which can be probed by label-free methods such as those based on microcantilevers,[41] goniometers,[42] or thin-film transistors. Importantly, these effects can complement those occurring in solution, thus allowing a better understanding of the whole process. Before introducing the thermodynamic tools that can allow a more complete picture to be gained of a biological process as it occurs in solution and on a surface, the most relevant immobilization processes of a protein are briefly reviewed.

2.1. Anchoring Biorecognition Elements to a Surface

The integration of biological recognition elements such as enzymes, antibodies, DNA, or whole cells on a transducing interface is a key step in the fabrication of many bioelectronic/biosensing platforms. The major requirement for achieving highly sensitive and selective transducers is the preservation of the integrity and activity of the biomolecules upon two-dimensional confinement. Ideally, biomolecules need to be immobilized onto solid surfaces in a high density and with a controlled orientation so as to provide good steric accessibility of the active binding sites to the affinity ligands. It is also important to limit nonspecific adsorption as well as to increase the stability. A variety of immobilization methods have been exploited to anchor biomolecules and are mostly based on physical adsorption, covalent binding, and bioaffinity coupling, with particular attention paid to site-specific deposition techniques.[43] The influence of external parameters such as temperature, ionic strength, and pH during the fabrication and operation of the device should also be considered, because they directly affect the conformation and the stability of the attached biorecognition elements. The most frequently used immobilization procedures for the integration of biomolecules in TFT devices are depicted in Figure 2.

Biomolecules can be adsorbed on a solid surface through hydrophobic, electrostatic, and/or ionic interactions.[44] This makes physical immobilization (Figure 2a) a simple route,

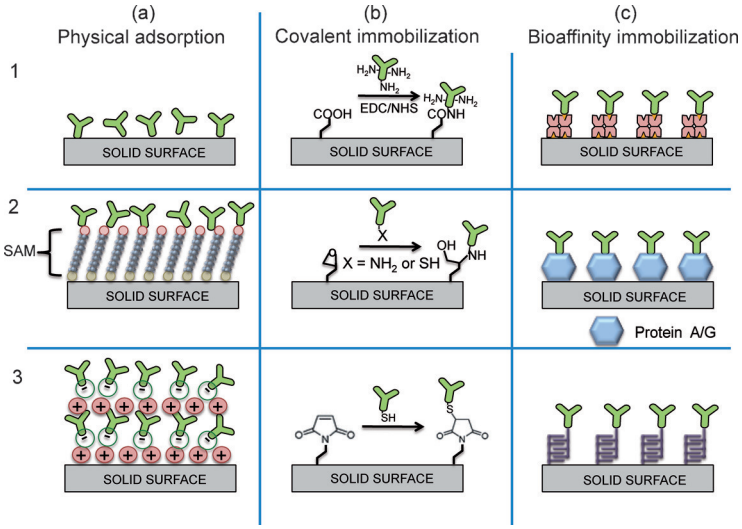

Figure 2. Methods for the immobilization of biorecognition elements on solid surfaces. (a) Physical immobilization techniques. Biomolecules are adsorbed on a bare surface (a1) or, to obtain a higher density, on a surface modified with a self-assembled monolayer (a2). Layer by layer adsorption (a3) by stepwise deposition of biological species having opposite charge is another way to control the immobilization of biomolecules on the surface. (b) Nonselective covalent immobilization of biomolecules through their functional residues. Biomolecules can be covalently anchored on a solid surface using: the reaction between carboxyl groups on the surface and the ammine groups of the lysine residues of the biomolecules upon activation of the carboxyl functionalities with carbodiimide hydrochloride (EDC) or *N*-hydroxysuccinimide (NHS; b1); the reaction between epoxides on the surface and nucleophilic residues such as amino or thiol groups of the biomolecules (b2); the reaction between maleimide groups on the surface and the thiol group of cysteine residues of the biomolecules (b3). (c) Bioaffinity immobilization reactions used for the orientation of biomolecules on a solid surface. Biotinylated biomolecules can be easily captured by a streptavidin layer deposited on the solid surface (c1) and vice versa. Surfaces coated with protein A or protein G can be used to specifically orient antibody molecules through binding with their fragment region that can be crystallized, Fc (c2). Biomolecules can be modified with a proper tag that is selectively recognized by specific molecules on the surface (c3).

particularly suited to deposit proteins on a variety of surfaces, including carbon-based materials, noble metals, and metal oxides. This method has also been exploited for the immobilization of DNA and proteins on the surface of organic semiconductors such as pentacene, poly(3-hexylthiophene-2,5-diyl) (P3HT), and PEDOT in TFT structures.[45] The main advantage of the physical adsorption is that neither additional coupling reagents nor chemical modification of the biomolecules are needed. However, the resulting biofilms usually lack homogeneity and are also weakly anchored to the surface; both these issues have an impact on the long-term stability of the device.

As an alternative, biomolecules can be stably anchored on a solid surface by covalent immobilization through the formation of chemical bonds between complementary functional groups present on the biomolecules and on the solid surface. Suitable functional groups are carboxyl, amine, and thiol functionalities (Figure 2b).[46] Although suitable functional groups are generally naturally present on the structure of the biomolecules, chemical linkers need to be introduced onto the solid support. Polymeric films or self-assembled monolayers (SAMs) bearing functional groups can be used for this purpose. Molecules in SAMs can have head groups such as thiols and disulfides and a variety of tail groups (-COOH, -NH_2, -CH_3) separated by alkyl chains of different length. The functional head group by itself or with subsequent chemical modifications enables fine tuning of the surface properties such as, hydrophilicity, cytophilicity, chemical resistance, and selective attachment of biomolecules in a preferential orientation.[47] In bioelectronic applications, carboxyl groups have been confined as anchoring sites on the surface of P3HT and pentacene semiconductors by depositing ultrathin hydrophilic polymeric coatings bearing -COOH functional groups by plasma-enhanced chemical vapor deposition.[48] The biomolecules can be covalently attached afterwards through carbodiimide chemistry, where the amino groups of the biomolecules form amide bonds with carboxyl groups present on the polymeric surface. Importantly, a finely tuned plasma process has been shown to have a negligible impact on the electrical performance of the EG-TFT.[49] Another proposed approach involves the chemical tailoring of the organic semiconductor by adding carboxyl moieties to the polymer backbone. A polythiophene-based semiconductor having carboxyl side chains has been used to covalently anchor DNA molecules in an EG-TFT structure.[50] However, the presence of polar groups in the bulk of the semiconductor may have an impact on the charge delocalization in the semiconductor and eventually on the electrical performance of the transistor. Blend systems have shown better performances when operated as electrochemical TFTs.[51]

Bioaffinity binding approaches (Figure 2c) provide advantages over other immobilization methods since biomolecules are precisely oriented on a surface and can be attached with high density.[52] Among them, the (strept)avidin–biotin system is the most widely exploited to immobilize oriented biomolecules on a variety of surfaces. Specifically, the strong noncovalent (strept)avidin–biotin biological interaction (dissociation constant $K_D = 10^{-15}$ M, fM) is used to bind biotinylated molecules on (strept)avidin-modified surfaces or vice versa. For example, supported biotinylated phospholipid layers, covalently attached to hydrophilic polymeric coatings deposited on the P3HT PSC surface by a plasma process, have recently been proposed to anchor biotinylated antibody through a (strept)avidin bridge in a EG-TFT.[53] Furthermore, a synthesized polythiophene copolymer with biotinylated side chains able to capture (strept)avidin molecules has also been proposed for use in EG-TFTs.[54] Very recently, genetically engineered chimeric avidin molecules containing C-terminal cysteine groups have been immobilized directly on the gold surface. The formed biolayer offers a higher binding capacity of the biotinylated molecules compared to wild-type avidin anchored on the same surface.[55]

2.2. Binding Isotherms at Surface-Confined Biomolecules

The adsorption of a species A on a solid surface can be modeled at the lowest level of complexity by the Langmuir adsorption isotherm.[56] This model describes the surface as an ensemble of fixed and independent adsorption sites that can be either empty (S) or occupied by the adsorbed molecule (Ad). Such a system is illustrated in Figure 3a along with the

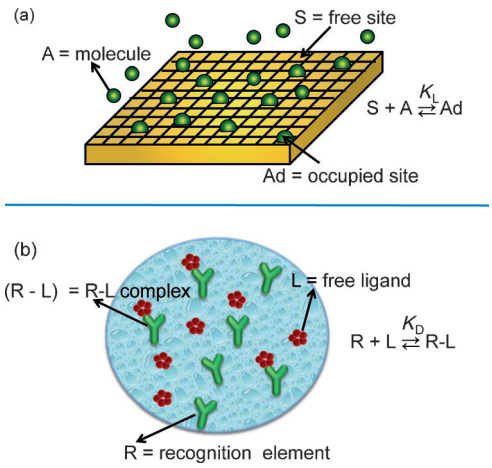

Figure 3. (a) Adsorption process of a molecule to a surface; (b) binding process in solution.

adsorption equilibrium reaction. The adsorption isotherm relates the fraction θ of sites occupied by the adsorbed molecules, $\theta = \mathrm{Ad}/(\mathrm{S} + \mathrm{Ad})$, to the concentration of A at equilibrium ($[\mathrm{A}]_e$), where K_L is the Langmuir constant, that is, the equilibrium constant for the adsorption process [Eq. (1a)].

$$\theta = \frac{[\mathrm{A}]_e}{\frac{1}{K_L} + [\mathrm{A}]_e} \tag{1a}$$

A very similar equation is obtained when considering the binding of a ligand L to a biological recognition element R dispersed in solution to form the R-L complexes, as depicted in Figure 3b. For the sake of simplicity, here we consider only one binding site per recognition element [Eq. (1b)].

$$\theta = \frac{[L]_e}{K_D + [L]_e} \quad (1b)$$

In this case, the equation corresponds to a binding isotherm for independent sites, with θ being the fraction of occupied binding sites, that is, $\theta = \text{R-L}/[\text{R} + (\text{R-L})]$. $[L]_e$ denotes the equilibrium concentration of the ligand L, while K_D is the dissociation constant, that is, the reciprocal of the equilibrium constant for the binding process. Despite the formal similarities between Equations (1a) and (1b), K_D and K_L^{-1} refer to different physical quantities. The dissociation constant K_D is defined as the ratio between the activities of the involved species in solution, namely R, L, and the complex R-L. At sufficiently high dilution, K_D can be approximated as [R]-[L]/[R-L] which is equivalent to saying that the standard state of all the species is chosen in solution according to the Henry convention. The Langmuir constant involves the activity of species, such as S and Ad, which are confined to a surface. Even at very low concentration of A (infinite dilution), K_L cannot be approximated using only the solution concentrations, their surface density should at least be used for the adsorption sites.

The numerical values of K_D or K_L^{-1} can be determined by measuring θ (or a property proportional to θ) as a function of the equilibrium concentration of A or L, $[A]_e$ or $[L]_e$, respectively, and fitting the data to Equations (1a) and (1b), respectively. The chosen scale of the concentrations implicitly sets the units of measure for K_D or K_L^{-1}. In the case where only the initial concentration, $[A]_0$ or $[L]_0$, is known, the amount of bound molecule must be taken into account explicitly. In the case of ligand binding in solution, the equilibrium ligand concentration is $[L]_e = [L]_0 - \theta([\text{R-L}] + [\text{R}])$, which leads to a quadratic solution for θ in Equation (1b). In the case of the adsorption process, an analogous relation must be written that takes into account that it is the surface density of empty (S) and occupied (Ad) binding sites that governs the process. An interesting example of this approach is provided in Ref. [27b].

A real ensemble of biological recognition elements can generally be described as a homogeneous system because the differences in the affinity constants among the R molecules are usually negligible. Thus, Equation (1b) typically gives a suitable description of the binding process in the case of single as well as independent binding sites. The adsorption sites of a real solid surface are, in contrast, generally characterized by different adsorption energies and, therefore, different Langmuir constants.

The overall adsorption isotherm for such an inhomogeneous system is obtained by integrating Equation (1b) over all the K_L values.[57] When multiple binding sites on the same recognition element occur, another phenomenon connected with inhomogeneity can emerge. The ligand affinity for a binding site, characterized by a given K_D value, can depend on the occupancy of the other binding sites present on the same biological recognition element. In such a case, the binding is said to be cooperative. In the case of positive cooperativity, the presence of occupied binding sites makes further ligand binding favorable. In the case of negative cooperativity, the binding to a site reduces the affinity of the ligands for the other sites. The case of strong cooperativity is described by the Hill model for a receptor with m binding sites.[58] If the binding is highly cooperative, R will bind/release exactly m ligands at a time according to the dissociation equilibrium [Eq. (2a)]. The fraction of occupied binding sites can be described by [Eq. (2b)].

$$\text{R-L}_m \overset{K_D}{\rightleftharpoons} \text{R} + m\text{L} \quad (2a)$$

$$\theta = \frac{[L]_e}{K_D + [L]_e} \quad (2b)$$

This is the Hill binding isotherm and is widely used to describe cooperative ligand binding to biological macromolecules. Whereas Equation (2b) returns Equation (1b) when $m = 1$, when $m > 1$ it models the case of positive cooperativity while $m < 1$ indicates a negative cooperativity. Since lateral interactions can also have a non-negligible impact on the adsorption on solid surfaces (positive or negative influence of adsorbed molecules on the adsorption of further molecules) it is possible to also find cases of cooperative adsorption on solid surfaces.[59]

2.3. Thermodynamic Transformations To Bring Biomolecules from Solution to Surface

It is not common to find thermodynamic studies that allow the properties of binding process taking place in solution and at a surface to be correlated. Such an approach allows the processes occurring in a bioelectronic device to be modeled and to gain a more complete view of a given binding process. The comparison between the binding equilibria involving species either confined at a solid–liquid interface or occurring in the bulk of a solution can be performed by considering the thermodynamic path reported in Figure 4.

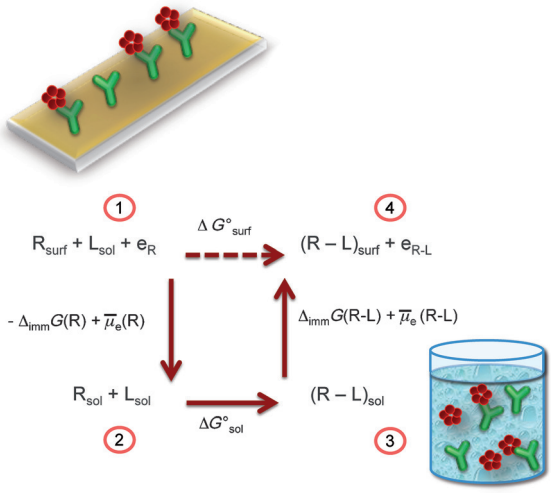

Figure 4. The thermodynamic path describing binding equilibria involving species either confined at a solid–liquid interface or in the bulk of a solution.

The overall process starts with a ligand L, dissolved in a solution, that binds to a surface-immobilized recognition element R (state 1) to form an immobilized complex R-L (state 4). The corresponding change in free energy $\Delta G°_{surf}$ can be described in terms of an apparent dissociation constant $K_{D,surf}$ as $\Delta G°_{surf} = RT\ln(K_{D,surf})$. It should be noted that $K_{D,surf}$ strictly has the meaning of K_L^{-1} in Equation (1a). The process (1→4) can be broken down into three possible steps, each being characterized by a change in the standard molar Gibbs energy. The first step (1→2) comprises the release of the recognition element R bound to the surface into the solution. The change in free energy associated with this stage encompasses the work needed to release R, which is opposite to the surface work $\Delta_{imm}G(R)$ required to immobilize it. Such work will depend on the strategy used to immobilize the R species, which will determine aspects such as the surface density or orientation of R. Since in the following we will be interested in recognition species anchored on a metallic gate (Figure 1c) or on the surface of a printable semiconductor (Figure 1d), the change in the electrochemical potential $\overline{\mu}_e(R)$ of the gate or of the PSC electrons also has to be considered. This allows the impact of the deposition or removal of the R layer on the electrostatics of a given surface to be taken into account. The second step (2→3) is the binding of L to R in solution, with a free energy change of $\Delta G°_{sol} = RT\ln(K_{D,sol})$ that is a function of the dissociation constant in solution. The final step (3→4) is the immobilization of the R-L complex to the gate or to the PSC surface with a change in the free energy, including the surface work spent on immobilizing the complex $\Delta_{imm}G(R\text{-}L)$ and the change in the metal-gate potential or in the PSC electron electrochemical potential $\overline{\mu}_e(R-L)$.

Following the scheme shown in Figure 4, the standard molar Gibbs energy for the surface binding of the biological recognition elements anchored to a surface can be written as Eq. (3).

$$\Delta G^0_{surf} = \Delta G^0_{sol} + \overline{W} = \Delta G^0_{sol} + \Delta E_F + W \tag{3}$$

Herein, the binding surface work $\overline{\mu}_e(R)$ is composed of a non-electrostatic term $W = \Delta_{imm}G(R\text{-}L) - \Delta_{imm}G(R)$ and an electrostatic term $\Delta E_F = \overline{\mu}_e(R-L) - \overline{\mu}_e(R)$. The latter is the change in the gate potential or in the electrochemical potential of the PSC electrons $\overline{\mu}_e$ as the surface changes from being coated with the R-L complex to the bare R layer. This ΔE_F value can be computed as the opposite of the molar free energy associated with the shift in the transistor threshold voltage (V_T) of the TFT, so that $\Delta E_F = -nF\Delta V_T$. It is important to outline that the latter equation holds true when no net charges are involved in the R-L interaction and for a trap-free TFT. V_T (defined in the next paragraph) accounts for the electrostatic built-in potential at the biological interface. ΔV_T is taken as the difference between the V_T values measured at zero ligand concentration (no binding site occupied) and at saturation (all the binding sites occupied), F is a molar quantity, so ΔE_F is the electrostatic contribution to the molar free energy for formation of the R-L complex.

It is also interesting to consider the use of Kelvin probe force microscopies to measure the electric potential, without physical contact, between the tip and the system to be studied at nanoscale resolution. These measurements exploit long-range electrostatic interactions between the scanning probe and the sample.[60a] and have been successfully used mainly to study charged species.[60b,c]

The binding energy in solution $\Delta G°_{sol} = RT\ln(K_{D,sol})$ is defined as the difference in the standard free energy between the complex R-L and the reagent partners R and L. The $\Delta G°_{surf}$ term is the change in the free energy between states 4 and 1, and is an electrochemical energy as it also includes an electrostatic component. The overall surface work $\overline{W}$ associated with the R-L binding encompasses the change in the physicochemical properties of the surface such as the interfacial tension, described by the W term, and the electrochemical potential of the electrons, described by ΔE_F.

According to Equation (3), the surface binding energy ($\Delta G°_{surf}$) can be split into a term that takes into account the molecular interaction energy ($\Delta G°_{sol}$) and one accounting for the surface work contribution ($\overline{W}$). Importantly, the molecular interaction term is the R-L recognition energy in solution. The surface work contribution describes the work carried out to accommodate the ligand into the recognition element that is bound to a surface. This term includes the conformational rearrangements as well as the change in the energy of the gate or of the electrochemical energy of the PSC, and Equation (3) can be also written as Equation (4).

$$\frac{K_{D,surf}}{K_{D,sol}} = e^{\frac{\overline{W}}{nT}} \tag{4}$$

This equation indicates that the affinity observed in solution will match that found for immobilized receptors only when the surface work $\overline{W}$ is zero, that is, when the work associated with the immobilization of the free recognition element R and of the R-L complex has the same value. In the more general case of non-negligible net surface work, this term will exponentially affect the ligand affinity for the immobilized biological recognition element.

A pretty spectacular example illustrating the key role that the surface work can play is given for the case of the hybridization of single DNA strands anchored to a solid surface. Many data are available as this is a widely exploited recognition reaction in many biosensor microarrays, including ELISA and SPR ones. The equilibrium constants for DNA hybridization taking place in solution and on a surface (for the same DNA sequences and under the same experimental conditions) have been systematically compared, as reported in Figure 5. The dashed line denotes the prediction for $K_{D,sol} = K_{D,surf}$. This condition is clearly never fulfilled; instead, the data points are widely spread. The surface hybridization constant changes by five orders of magnitude while the same quantity spans over thirty orders of magnitude in solution. The experiment data were gathered by systematically changing the salinity of the electrolyte solution and the DNA sequence. Eventually, it is seen that the $K_{D,surf}/K_{D,sol}$ ratio spans over a huge range of about 27 orders of magnitude.[61] According to Equation (4), the surface work $\overline{W}$ should account for such an occurrence. This hypothesis was subsequently tested by actually measuring the mechanical

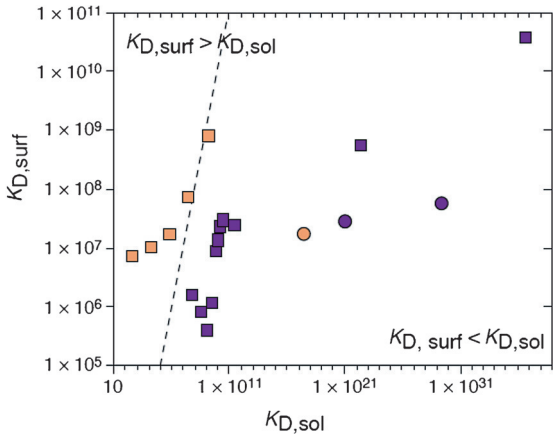

Figure 5. Comparison of equilibrium constants for DNA hybridization processes taking place at a solid surface ($K_{D,surf}$) and in the bulk of a solution ($K_{D,sol}$). Figure adapted from Ref. [60] and reproduced with permission, Copyright 2005, Elsevier Ltd.

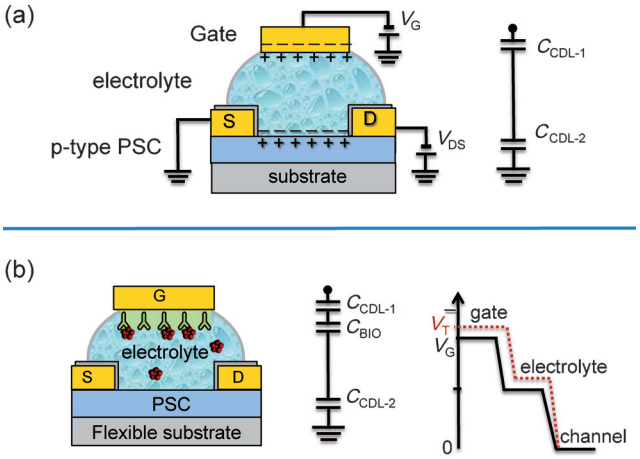

Figure 6. (a) Electrolyte-gated TFT along with a series of electrical layer capacitors that form the conducting dielectric; (b) Bioelectronic EG-TFT along with the series of capacitors that form the gating system of the device and the potential drops occurring across the electrolyte.

contribution to the surface work associated with DNA hybridization by means of a microcantilever set-up.[62] It was found that W can indeed range between $-90\ kJ\,mol^{-1}$ and $+75\ kJ\,mol^{-1}$. Upon substitution of these values into Equation (4) (neglecting the electrostatic contribution that cannot be evaluated by a cantilever), a $K_{D,surf}/K_{D,sol}$ ratio ranging from 10^{-16} to 10^{+13} can be obtained. This ratio spans over 29 orders of magnitude, and is very close to the data evaluated by directly comparing the dissociation constants.

3. Printable Bioelectronic Electrolyte-Gated Thin-Film Transistors

The first demonstration that an electrolyte could be employed to adjust the surface potential of a semiconductor can be traced back to the early days of transistors at the Bell laboratories.[63] Nowadays, many groups are working on EG-TFTs in which printable semiconductors are employed as the active layer.[7a,64] As already introduced, the structure of an EG-TFT comprises a source and a drain contacts on a substrate and covered by a semiconductor, generally deposited by printing-compatible techniques. A droplet of pure water or of an electrolyte is placed on the surface of the semiconductor. The PSC surface can be hydrophobized by suitable treatments if the surface contact angle is too small and/or the semiconductor is soluble in water, such as ZnO. In this case a treatment with hexamethyldisilazane has been proposed.[65] The electrical contact to the gate is made through a metal plate (usually gold) placed on top of the electrolyte. A p-type TFT is operated by applying negative V_{DS} and V_G biases to the drain and the gate contacts, respectively, while the source contact is grounded (Figure 6a). After application of V_G, the electrolyte ions redistribute so that the cations face the negatively biased gate plate, while the anions align at the semiconductor surface. Pure water can also act as an ionic conductor as a result of self-ionization. Charge double layers (CDLs) at the gate/electrolyte and electrolyte/semiconductor interfaces, termed C_{CDL-1} and C_{CDL-2}, respectively, in Figure 6a, eventually form, which hold capacitances as high as $14.6\ \mu F\,cm^{-2}$ in 0.1 M saline solution.[66] Capacitance values up to hundreds of $\mu F\,cm^{-2}$ can be obtained using ionic liquids and polymeric electrolytes as a result of the much higher ionic concentrations.[67] The two CDL capacitors in series, reported in Figure 6a, form an EG-TFT gating system as the capacitance coupling between the CDLs and the semiconductor generates a two-dimensional (2D) channel of free charges in the semiconductor.[68] These charges are injected and can drift under the V_{DS} bias. However, when V_G is applied, the conditions for the 2D accumulation of free charge at the semiconductor/electrolyte interface are set, but the actual source–drain current (I_{DS}) in the semiconductor flow does not start (under a given applied V_{DS}) until V_G equals the threshold voltage V_T of the TFT. In a trap-free TFT, V_T is the bias needed to offset the built-in potential generated by the mismatch existing between the gate metal and the semiconductor free electrons $\overline{\mu}_e$. As V_G equals V_T, the energy barrier is flattened and, beyond V_T, further injected charges can drift under the influence of the applied V_{DS} through the channel with a given field-effect mobility (μ_{FET}), and the transistor output characteristics (I_{DS} versus V_{DS}) can be measured. Each applied gate bias (subtracted from the V_T component) sets the density of charges that are induced in the transistor 2D channel and, therefore, also the maximum I_{DS} current intensity.[20] As a result of the very high capacitance of the EG-TFT electrolyte, the transistor current–voltage output characteristics, which show the expected linear (at lower V_{DS}) and saturation regimes, can be measured by biasing the device below 1 V.

A bioelectronic version of the EG-TFT is shown in Figure 6b along with the series of capacitors associated with the gating system as well as the potential drops across the electrolyte. In this configuration, the capacitance per unit area of the biological layer (C_{BIO}) attached to the gate electrode is added. C_{BIO} is modeled as a planar capacitor, $C = \varepsilon_0\varepsilon_r d^{-1}$, with ε_0 and ε_r being the vacuum and the relative permittivity, respectively, while d is the distance between the

capacitor plates. Taking $\varepsilon_r = 3$, typical for a protein system,[69] and d as the height of a monolayer of proteins (ca. 4 nm for the case of odorant binding proteins discussed later), a C_{BIO} value of 0.6 μF cm^{-2} is estimated.

The I_{DS} current flowing in the 2D channel in the saturation regime is given by Equation (5), where C_i is the capacitance per unit area of the EG-TFT gating system, while w and l are the width and the length of the TFT channel, respectively.[20]

$$I_{DS} = \frac{w}{2l} C_i \mu_{FET} (V_G - V_T)^2 \quad (5)$$

Equation (5) describes well the experimental I–V curves measured with an EG-TFT. A typical example is shown in Figure 7.[70] Here, the I--V curves of an α-sexithiophene organic semiconductor, interfaced to an aqueous electrolyte containing 10 mM K-based phosphate buffer saline (PBS), adjusted to an ionic strength of 50 mM with KCl, are reported. Such an EG-TFT device is proposed by the authors as a pH sensor. Figure 7a clearly shows that EG-TFT I–V curves can be measured by sweeping V_{DS} between 0 V and −0.6 V as a consequence of the high capacitance of the CDLs that result in a large TFT transconductance. Moreover, the characteristic curves of the device exhibit the typical behavior of a field-effect device, with a saturation regime at higher drain–source voltages, as described by Equation (5). Figure 7b shows how I_{DS} decreased by less than 10% during continuous cycling of V_{DS} for more than 3 h. This is convincing evidence that EG-TFT devices can also be quite stable. It is foreseen that even better stabilities could be obtained if, instead of a continuous bias, a pulsed mode of operation is used.[71]

It has also been demonstrated recently that printable EG-TFTs can be realized on a multilayer-coated paper substrate and operated with an ionogel-based electrolyte. Such ionogels are produced by gelation of microcellulose thin films with tailored 1-ethyl-3-methylimidazolium methylphosphonate ionic liquids, and exhibit capacitances as high as 5 to 15 μF cm^{-2}.[10] Interestingly, the TFT structure with a spray-coated ZnO layer (Figure 8a) reached a μ_{FET} value as high as 75 cm^2 V^{-1} s^{-1}. Moreover, solution-processed colloidal ZnO nanorods coupled to laminated cellulose ionogels has enabled the fabrication of the first electrolyte-gated, flexible circuits on paper, which operate at a bending radius down to 1.1 mm. A rather stable operation is seen after bending more than 100 times. Pictures of the device also under bending are shown in Figure 8b,c, while the I–V transfer characteristics of the device and performance features are reported in Figure 8d–f.

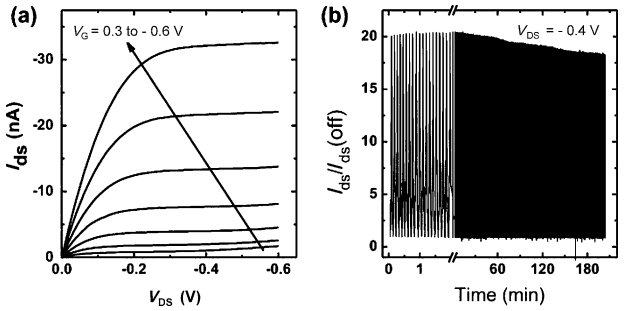

Figure 7. (a) EG-TFT output characteristics of an α-hexylthiophene TFT gated though an aqueous electrolyte with a phosphate-buffered potassium saline solution. The gate voltage V_G was applied between a Ag/AgCl reference electrode and the source contact of the transistor. (b) Recording of the drain current during continuous cycling of the device between the on state ($V_G = -0.6$ V) and the off state ($V_G = 0.3$ V). Figure adapted from Ref. [70] and reproduced with permission, Copyright 2011, AIP Publishing LLC.

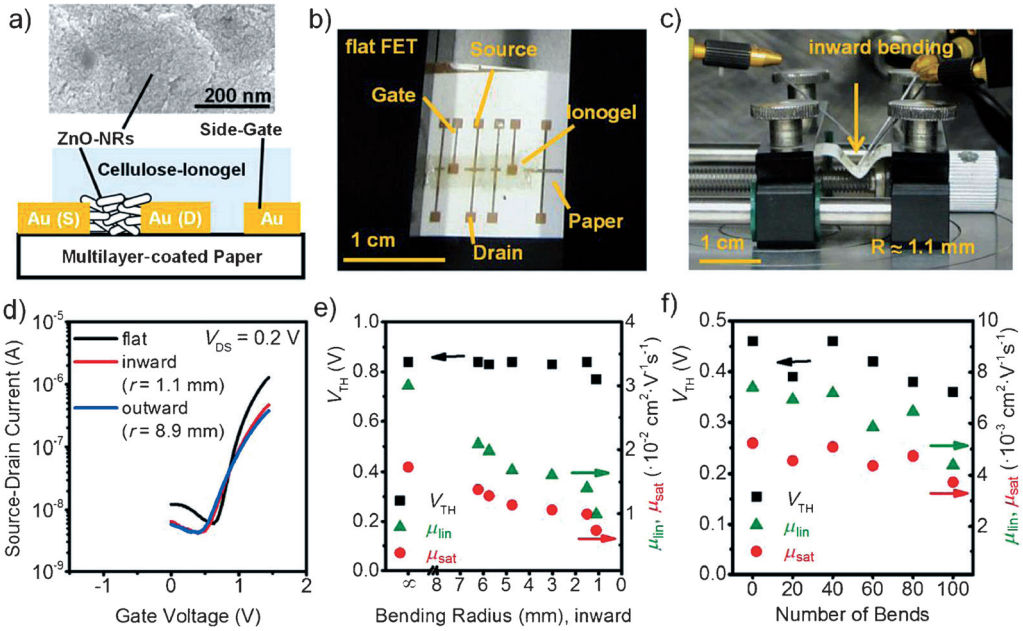

Figure 8. (a) Schematic illustration of an electrolyte-gated TFT with ZnO nanorods and a side gate on multilayer-coated paper with laminated cellulose ionogel. Inset: SEM image of ZnO nanorods (length 14 nm) on paper. (b) Optical image of a TFT with ZnO nanorods on multilayer-coated paper with laminated ionogel before bending and (c) during inward bending with a bending radius of 1.1 mm. (d) Transfer characteristics before and during inward (radius 1.1 mm) and outward bending (radius 8.9 mm) at $V_{DS} = 0.2$ V. (e,f) Threshold voltages and linear and saturation electron-field-effect mobilities versus bending radius (e) and versus number of bends (bending from flat to a bending radius of 1.1 mm; f) for ionogel-gated TFT with ZnO nanorods on a multilayer-coated paper substrate in a nitrogen atmosphere. Reproduced from Ref. [10] with permission, Copyright 2013, Wiley-VCH, Weinheim.

3.1. The Impact of Biological Recognition on TFT Performance Features

The response of a bioelectronic TFT can be conveniently evaluated by measuring the device transfer characteristics, namely the I_{DS} versus V_G curve at a constant V_{DS} value in the saturated region. According to Equation (5), $\sqrt{I_{DS}}$ is linear in $(V_G - V_T)$, as depicted by the plots in Figure 9 for different bioelectronic TFT structures.

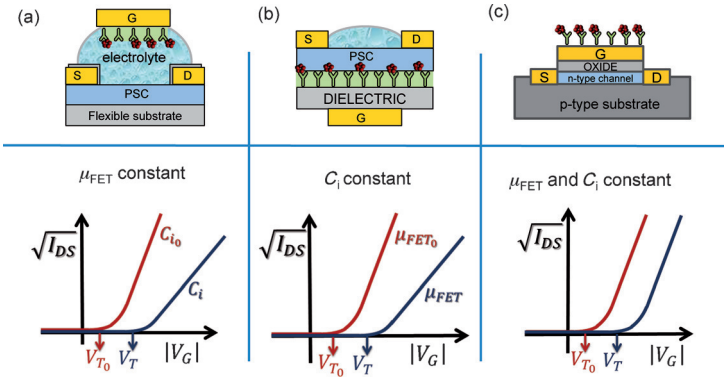

Figure 9. Representation of the transfer characteristics of different bioelectronic TFTs before and after a binding event. (a) In an EG-TFT, the device is modulated by the capacitance of the biolayer. (b) In the FBI transistor, the gating capacitance is constant and both μ_{FET} and the V_T change. (c) In an ISFET, only V_T changes.

A linear interpolation allows easy extraction of the TFT performance features: $(C_i \cdot \mu_{FET})$ is proportional to the slope of the $\sqrt{I_{DS}}$ versus V_G curve, while V_T is the intercept with the abscissa (V_G). In general, if the semiconductor transport is affected by the formation of the R-L complex, μ_{FET} will change; when the complex formation has an impact on the gating capacitance, C_i will be affected. If the impact is to the free electrons $\overline{\mu}_e$ of the semiconductor or of the gate metal, then V_T shifts. These three occurrences can take place contemporarily, but the cases where these effects can be decoupled are interesting to study, as shown for the device structures reported in Figure 9. In the following, we explicitly refer to the case of a biosensor that probes the binding of ligand to an immobilized biomolecule, but the same arguments hold for a device probing the nonspecific absorption of a ligand on a solid (PSC or gate) surface.

For bioelectronic TFTs, C_i is the result of at least three capacitances in series, as shown in Figure 6b, and therefore it can be written as: $1/C_i = (1/C_{CDL\text{-}1} + 1/C_{BIO} + 1/C_{CDL\text{-}2})$. If one of the contributing capacitances is much lower than the others, C_i can be approximated to this value. In this respect, the case of the EG-TFTs (Figure 9a) is a peculiar one. Indeed, the highest capacitances of the series are those of the gate/electrolyte Helmholtz double layers ($C_{CDL\text{-}1}$), which can reach tens of $\mu F\,cm^{-2}$, while the C_{BIO} value can be about 0.5–0.6 $\mu F\,cm^{-2}$ and the electrolyte/PSC double layer capacitance ($C_{CDL\text{-}2}$) a few $\mu F\,cm^{-2}$.[64b] Therefore, the lowest capacitive contribution to the TFT gating system comes from the layer of biological molecules. Eventually, it is the C_{BIO} contribution that drives or modulates the output current of the EG-TFT. As the dielectric properties of the R layer will change upon the binding of L, the EG-TFT can be very sensitive to subtle changes connected with the conformational changes, even when no net charges are involved. At the same time, the mobility of the semiconductor will remain constant (particularly for the case where the biolayer is deposited on the gate), while V_T can effectively transduce the electrostatic component of the R-L interaction.

Comparison with a bottom gate FBI transistor and with an ISFET is interesting. In an FBI transistor (Figure 9b), the hundreds of nm thick SiO_2 insulating dielectric (capacitance in the $nF\,cm^{-2}$ range) typically present is by far the lowest contribution to the capacitance series and, therefore, in this case it is the insulating dielectric capacitance (which will not change upon binding) that gates the device. Therefore, as a consequence of the proximity between the biolayer and the semiconductor 2D channel in FBI transistors, μ_{FET} is affected by the binding process, while the capacitance stays constant. This configuration is ideal for studying the effect of changes to the biolayer on the semiconductor transport, while V_T, as a consequence of its nature, will transduce the electrostatic component of the interaction. In ISFETs, the low capacitance of the oxide dielectric (Figure 9c) also dominates in the capacitors series. In this MOSFET, the gate is modified with the biolayer and, upon interaction with a ligand, neither μ_{FET} nor C_i will change, the former as there is no contact between the biolayer and the semiconductor, the latter because of the low capacitance of the inert oxide layer. In this case, a shift in V_T is only measured as an effect of the change to the gate electrons $\overline{\mu}_e$. This is the reason why ISFETs, as well as charge-modulated transistors, are generally used only for the detection of charged species.

The relative variation of the saturated current I_{DS} $(\Delta I/I)$ is a robust parameter that can be taken as the bioelectronic TFT response because it normalizes the device-to-device variation, thus contributing to obtaining a highly reproducible response. $\Delta I/I$ also allows the contributions coming from the different performance features to be separated when second-order terms are neglected. Under this assumption, $\Delta I/I \approx [\Delta\mu_{FET}/\mu_{FET} - 2V_T/(V_G - V_T)]$ for the FBI device, while it is $\Delta I/I \approx [\Delta C_i/C_{i,} - 2\Delta V_T/(V_G - V_T)]$ for an EG-TFT with C_i being dominated by the capacitance of the biolayer. The full expression for the EG-TFT becomes Equation (6).

$$\frac{\Delta I}{I} = \frac{\Delta C_{OBP}}{C_{OBP}} - 2\frac{\Delta V_T}{(V_G - V_T)} - 2\frac{\Delta C_{OBP}}{C_{OBP}}\frac{\Delta V_T}{(V_G - V_T)} \quad (6)$$

If $V_T \ll V_G$ and $\Delta V_T \ll V_G$, Equation (6) becomes: $\Delta I/I \approx \Delta C_i/C_i$. This shows that an EG-TFT can actually be operated as a capacity-modulated transistor, which is particularly suited to the study of interactions occurring between biological species that do not bear a net charge. Moreover, the output current of the EG-TFT can be modulated by the change in the capacitance of the biolayer and, strikingly, this would work better when the changes in capacitance are small.

Therefore, in a TFT modulated by the biolayer capacity, all the capacitances that are in series with the biolayer one, become less and less effective as the biolayer capacitance (and its changes) becomes smaller and smaller. This holds true, provided parallel parasitic capacitances are kept low. This can be viewed as a "reverse" concept in the detection of biological species, and can be ideal for sensing ultralow concentrations. At the same time, a thermodynamic study will give access to the changes in free energy, thereby allowing for a holistic approach to study the binding properties of interfacial proteins. The case of odorant binding proteins confined on the gate and which interact with the enantiomers of carvone odorant molecules is an interesting example that will be discussed in the following section.

3.2. The Role of the Capacitance in the Mechanisms of Bioelectronic Electrolyte-Gated Transistors

The overall response in a bioelectronic device reflects the peculiar energetic aspects associated with a process involving recognition elements adsorbed on a surface that form a complex with an affinity ligand. A recent example[6] involving porcine odorant binding proteins (pOBPs) clarified the complexity of this interplay. pOBPs are small proteins, found in the nasal mucus of vertebrates or the sensillum lymph in the antennae of insects, that have a single binding site to host nonhydrophilic ligands. Their binding properties are characterized by a broad selectivity to a range of odorant ligands with dissociation constants in the μM range. The pOBP-mutant F88W was shown to be active in a competitive fluorescent binding assay performed in solution. The assay gave dissociation constants $K_{D,sol}{}^{+}$ for the pOBP–carvone complexes (pOBP-C) of 0.5 μM and $K_{D,sol}{}^{-}$ of 1.2 μM, for (*S*)-(+)- and (*R*)-(−)-carvone, respectively, and the detection limits were also evaluated to be in the sub-μM range. The data were successfully modeled using Equation (1a), thereby proving the occurrence of a non-cooperative binding process for the two carvone enantiomers in solution. The same assay was performed using an EG-TFT configuration. Although pOBPs are weakly negatively charged in pure water, (*S*)-(+)- and (*R*)-(−)-carvone enantiomers are odorant molecules that bear a dipole moment rather than a net charge. This occurrence does not make them a privileged choice for detection by a transistor, as charged species lead to a larger output response. However, as will be shown in the following, in this case the changes in capacitance will give rise to a large variation in the signal, which will allow chiral species to be differentially detected at the pM level.

Figure 10a shows a schematic representation of an EG-TFT structure with integrated pOBP molecules. The PSC is a poly[2,5-bis(3-tetradecylthiophen-2-yl)thieno[3,2-*b*]thiophene] (PBTTT-C14) p-type layer deposited on a flexible substrate, while the electrolyte is water. The gold-gate plate was functionalized with a very compact pOBP SAM. Specifically, the carboxy groups were grafted onto the electrode surface by means of a solution of 3-mercaptopropionic acid. The pOBPs were then covalently attached to the surface through carbodiimide chemistry. This gate was then placed on

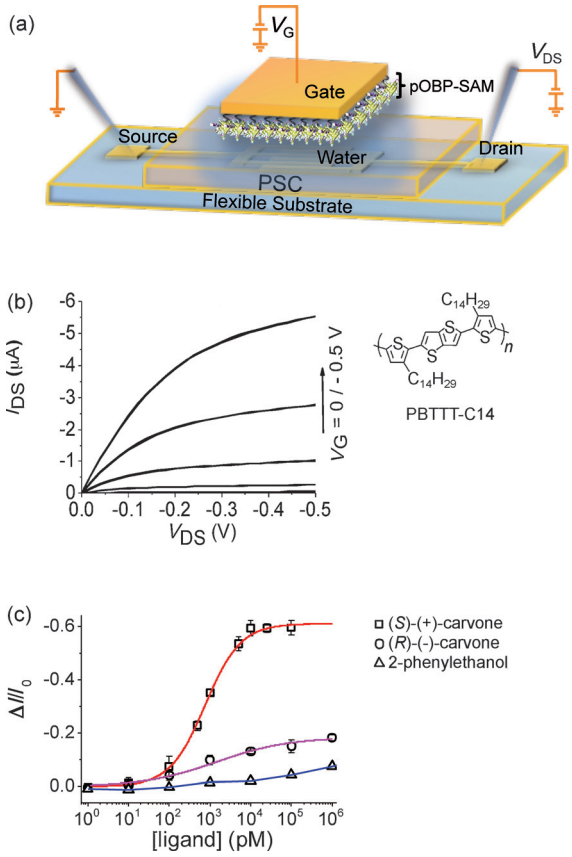

Figure 10. (a) WG-TFT based on a p-type PBTTT-C14. A biofunctionalized Au plate lies in contact with the water droplet, thereby acting as a gate. (b) The *I*–*V* curves are measured in the common-source mode with V_{DS} scanned between 0 and −0.5 V. The gate bias V_G varies in the same range in steps of −0.1 V. The measurements were performed by sweeping the drain voltage back and forth to evaluate the occurrence of any hysteresis. (c) Fractional changes in the capacitance as extracted from the source–drain current measured upon exposure to (*R*)-(−)- and (*S*)-(+)-carvone as well as 2-phenylethanol ligands in the 1 to 10^6 pM range. $\Delta I/I$ is the electronic response at a given concentration and the relevant dose–response curve is obtained by plotting these data points at all investigated concentrations as the average values over three replicates on different devices, with the relative error taken as one standard deviation. See Ref. [6] for more details.

the water droplet, which was already in contact with the PBTTT-C14 surface, and the *I*–*V* characteristics shown in Figure 10b were measured. The voltage was swept between 0 V and −0.5 V and a μ_{FET} value as high as 1×10^{-1} $cm^2 V^{-1} s^{-1}$ was extracted.

To study the pOBP–carvone binding, the fractional decrease in the output current of the pOBP EG-TFT upon carvone binding was evaluated. To this end, the I_{DS} versus V_G transfer curves have been measured in the absence (base line curve) and in the presence (signal curve) of the carvone molecules. $\Delta I/I = [(I - I_0)\, I_0^{-1}]$ is evaluated by taking I and I_0 as the I_{DS} values (at $V_G = -0.5$ V) of the signal and baseline values, respectively. The binding curves of the (*S*)-(+)-carvone and (*R*)-(−)-carvone ligands to the pOBP SAM are reported in Figure 10c as $\Delta I/I$ versus ligand concentration. The interaction with 2-phenylethanol was used as a negative control. The response curves to the carvone enantiomers are

distinguishable down to concentrations of a few tens of pM, thus showing that chiral species can be differentially detected at extremely low concentrations with an EG-TFT. The fitting of the (*S*)-(+)-carvone binding curve (red solid line in Figure 10b) is performed using the Langmuir isotherm [Equation (1a)], while that of the (*R*)-(−)-carvone (magenta solid curve in Figure 10b) could only be modeled using the Hill binding model [Equation (1b)], which was also used to model the data for 2-phenylethanol (blue curve). The fit of the (*S*)-(+)-carvone data to a Langmuir isotherm with non-cooperative binding gives a dissociation constant $K_{D,surf}{}^{+} = 0.8$ nM and limit-of-detection of 50 pM, while the quantification limit is 150 pM. The best-fit parameters for (*R*)-(−)-carvone are $K_{D,surf}{}^{-} = 20$ nM and $m = 0.5$ ($m < 1$), which suggests that an anti-cooperative binding occurs in this case. Hill's Equation also successfully accounts for 2-phenylethanol binding exhibiting an anti-cooperative behavior ($m = 0.3$). Thus, it can be deduced that the binding of the (*S*)-(+)-carvone ligand is non-cooperative when the pOBPs are anchored on a solid surface, as is the case for the binding of pOBP to both enantiomers of carvone in solution. An anti-cooperative behavior is seen for (*R*)-(−)-carvone, which suggests that the close packing of the proteins into a two-dimensional array allows lateral interactions to occur between the proteins, which affects the cooperativity. Such lateral interactions are absent in solution (as expected) and disappears when the confined pOBPs interact with (*S*)-(+)-carvone. This occurrence can be accounted for by a model of the pOBP layer that foresees a thin layer, maybe constituted by a few adsorbed water molecules, with a high dielectric that couples neighboring protein during the interaction with (*R*)-(−)-carvone. Interestingly, the model predicts that such a channel disappears when the protein interacts with (*S*)-(+)-carvone.[6] Such marked differences in the interaction mechanisms are most probably responsible for the extremely high enantioselectivity factor measured. This is taken as the ratio between the slopes of the linear branches of the binding curves, and is larger than 6, which is one of the highest measured, particularly at such an ultralow ligand concentration. Therefore, the binding of the two carvone enantiomers to the pOBP SAM, with markedly different levels of cooperativity and an exceptionally high enantioselectivity factor, provides evidence that markedly different interactions can indeed occur for surface-segregated biological recognition elements.

Besides evaluating the differences in binding properties, the pOBP EG-TFT binding study shows that the dissociation constants measured with the TFT ($K_{D,surf}$) are at least three orders of magnitude lower than those measured in solution ($K_{D,sol}$), while the scale of affinity is preserved. This is exactly what Equation (3) predicts and it is very interesting to compute the *W* values for both carvone enantiomers using the values measured for the binding free energies in solution and on the TFT as well as the shift of the device threshold voltage. In Ref. [6] it is shown that *W* has indistinguishable values for the two enantiomers, while a sizable difference is seen for the $\overline{W}$ electrochemical work. This means that the work to immobilize the complex would be independent from the chiral interaction, thus proving that it mainly involves the inner cavity of the pOBP. The data clearly suggest, therefore, that the $\Delta G°_{sol}$ term accounts for the inner cavity processes, while the surface electrochemical work is connected to the transistor transduction. These are quite important conclusions that can only be derived because of the more complete view of the formation of the pOBP–carvone complexes acquired by combining information that is measured in solution with a bioelectronic TFT.

The ability of an electrolyte-gated transistor to detect minute changes occurring in a protein layer is also supported by the work of other research groups. In this respect, the case of a graphene-based EG-TFT that integrates odorant receptors deposited on the graphene surface is quite interesting. The device structure is reported in Figure 11a.[72] The EG-

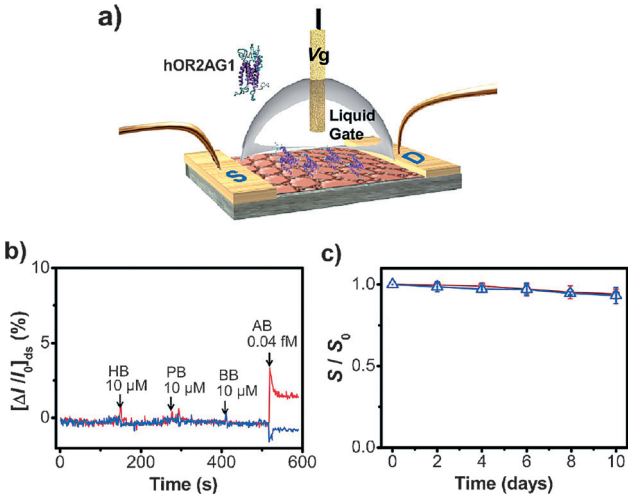

Figure 11. (a) Schematic diagram of an EG-TFT based on plasma-treated bilayer graphene conjugated with an olfactory receptor. (b) Selective responses of the graphene EG-TFT upon addition of hexyl butyrate (HB), propyl butylate (PB), butyl butyrate (BB), which are not target molecules, and of amyl butylate (AB), the target odorant. (c) Storage test of the EG-TFT. Figure adapted from Ref. [72] and reproduced with permission, Copyright 2012, American Chemical Society.

TFT relies on an electronic graphene layer whose surface is modified by grafting the human olfactory receptors 2AG1 (hOR2AG1). The graphene bilayer is subjected to a plasma treatment in a controlled oxygen or ammonia atmosphere to induce a stable p-type and n-type transport, respectively. The 1,5-diaminonaphthalene was then stacked on the plasma-treated graphene and linked to the odorant receptor through reaction with glutaraldehyde.

The hOR2AG1 is part of the G-protein-coupled receptor family and exists in two clearly identifiable conformational states: in one state, the cysteine residues are neutral, while in the other they are negatively charged. The specific interaction with odorants triggers a structural rearrangement of the odorant receptor, which leads to a marked switching to the negatively charged state.[73] In Figure 11b the I_{DS} transient traces of the hOR2AG1 EG-TFT exposed to different odorants are reported. The blue trace is for the n-type graphene while the red trace is for the p-type graphene. The

transistor was exposed to extremely low concentrations (0.05 fM) of an amyl butyrate (AB) ester odorant, which produces a perfectly measurable relative variation in the current of a few percent. The change in the current in opposite directions for the differently doped graphene surfaces is proof that the system reacts to the net negative charge that forms on the odorant receptor as it selectively interacts with the amyl butyrate odorant. No response can be measured when odors such as hexyl butyrate (HB) propyl butyrate (PB), and butyl butyrate (BB) are injected at much higher concentrations (10 μM). In this case, the odorant receptors do not undergo the conformational change that brings them into the charged state. The detection limit for the AB ester is reported to be as low as 0.04 fM with a signal-to-noise ratio of 4.2:1, while the equilibrium constants are in the 10^{-14} M range. Such an astonishingly low limit-of-detection further proves the potential of EG-TFTs can be extremely high and even enhanced when a net charge is generated upon binding. In this case, the system, although still being modulated by the changes in the capacitance of the biolayer, also takes advantage of the large electrostatic changes, which most probably sum up and result in a huge relative change in the current. The device was also shown to be very stable over 10 days, as shown by the data reported in Figure 11c.

Another example that shows the strength of the capacity-modulated EG-TFT detection is provided by the comparison of two different bioelectronic TFTs, both detecting dopamine (DA). In Figure 12a an EG-TFT whose gold gate contact is modified by a SAM of cysteamine and 4-formylphenylboronic acid, is reported.[74] This SAM enables the selective and covalent binding of dopamine, as a consequence of esterification of 4-formylphenylboronic acid with dopamine. Such a chemical reaction does not involve a charge transfer to the electrode. Instead, in the dopamine adsorption process, a large surface dipole builds up as a result of the zwitterionic structure of the boronic acid and the amine group. The transfer characteristics measured after exposing the gate to different dopamine concentrations clearly show that the device is capable of producing a large variation in current, even when a dopamine concentration as low as 1 pM is detected (Figure 12b). This is due to a dielectric and electrostatic change occurring in the SAM upon dopamine binding, although no electrochemical oxidation of dopamine takes place. Interestingly, nM sensitivity was achieved at best with an organic electrochemical transistor that exploits the oxidation of dopamine and gives rise to an increase in the faradaic current measured with the TFT.[75] A similar process is seen with the bioelectronic TFT reported in Figure 12c. In such a structure, the graphene layers act as both the channel and gate electrode.[76] The graphene gate also acts as the working electrode in the electrochemical process that leads to oxidation of the dopamine and to the transfer of an electron to the gate. The transient current I_{DS} in the presence of different concentrations of dopamine are reported in Figure 12d. The device shows a stable performance, but a dopamine concentration of 1 nM at best could be detected. A possible explanation to the apparently systematic lower detections achieved when an electrochemical reaction is involved is that, as is typical for a potentiometric electrochemical process, the double layer charging capacitive current competes with the faradic one during the detection. This capacitive component, being typically as high as 20 μF cm^{-2}, leads to a background transient current that can affect the detection limits of electrochemical TFTs. On the other hand, this is a very high capacitance that does not affect the resultant capacitance of the gating system of a EG-TFT.

4. Summary and Outlook

Electrolyte-gated thin-film transistors can be used as high-performance as well as printable bioelectronic devices. Examples of TFTs that involve organic semiconductors as well as solution-processed zinc oxide and graphene layers

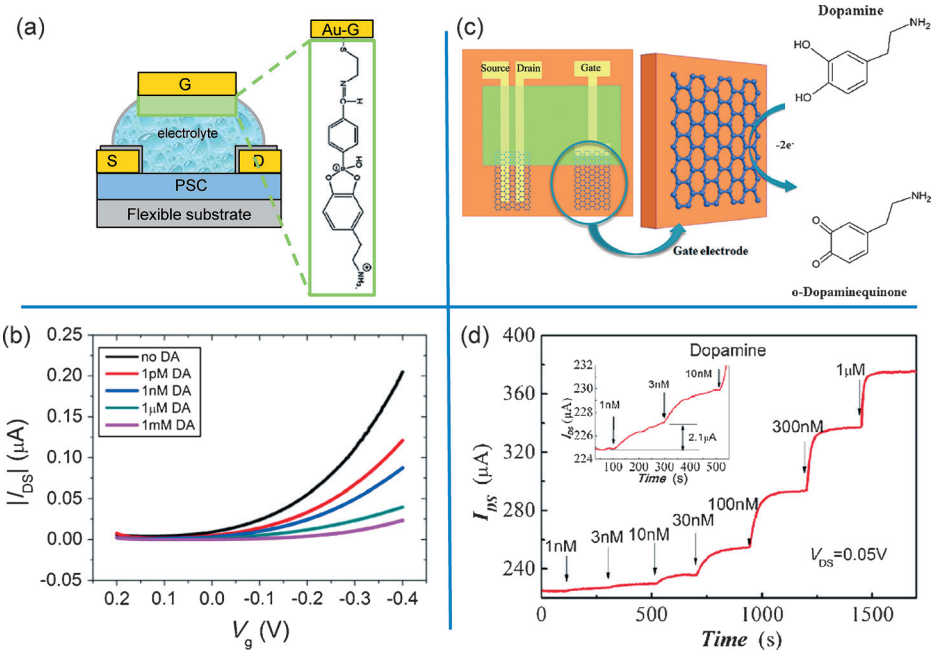

Figure 12. (a) Schematic representation of a device which indicates the gate electrode to be the active sensing surface along the chemical structure of the recognition element SAM on the gold surface. (b) Transfer curves for different dopamine concentrations. c) Schematic diagram of a graphene channel and an electrolyte-gated transistor with a graphene gate. The electrochemical reaction of dopamine on the graphene gate electrode is also described. (d) The channel transient current response of the transistor to additions of different concentrations of dopamine. V_{DS} = 0.05 V, V_G = 0.7 V. (a,b) Adapted from Ref. [73] and reproduced with permission, Copyright 2013, Elsevier B.V; (c,d) reproduced from Ref. [75] with permission, Copyright 2013, Wiley-VCH, Weinheim.

have been discussed. The devices have an integrated biolayer that is interfaced to either one of the electronic interfaces of the transistor. The key aspect of their functioning mechanism is the presence of high-capacitance charge double layers that allow very subtle changes occurring in the biolayer to be probed as the surface-confined recognition elements selectively interact with their affinity ligand. Differential detection of chiral species with large enantiomeric discrimination factors and accurate estimation of interaction energies as low as a few kJ mol^{-1} have been shown. These devices have also proven to be unique tools with general applicability that allow ligand detection in the sub-femtomolar concentration range. Such a technology holds the potential to revolutionize the present approach to point-of-care diagnostics. At the same time, a thermodynamic study involving changes in the free energy in solution and on the electrode gives access to a holistic approach to the study of the binding properties of interfacial proteins.

Krishna Persaud, Gianluca Lattanzi, and Paolo Bergese are acknowledged for useful discussions. The work discussed in this Review was produced thanks to financial support of the following proposal: PON project "Laboratorio per lo Sviluppo Integrato delle Scienze e delle Tecnologie dei Materiali Avanzati e per dispositivi innovativi -LABORATORIO SISTEMA", Sense-of-care-OFET biosensors for point-of-care applications—PITN-GA-2012–316845, OrgBIO—Organic Bioelectronics—PITN-GA-2013-607896.

How to cite: *Angew. Chem. Int. Ed.* **2015**, *54*, 12562–12576
Angew. Chem. **2015**, *127*, 12746–12762

[1] a) I. R. Minev, P. Musienko, A. Hirsch, Q. Barraud, N. Wenger, E. M. Moraud, J. Gandar, M. Capogrosso, T. Milekovic, L. Asboth, *Science* **2015**, *347*, 159–163; b) J. Rivnay, R. M. Owens, G. G. Malliaras, *Chem. Mater.* **2014**, *26*, 679–685; c) M. Berggren, A. Richter-Dahlfors, *Adv. Mater.* **2007**, *19*, 3201–3213.

[2] I. Willner, R. Baron, B. Willner, *Biosens. Bioelectron.* **2007**, *22*, 1841–1852.

[3] D. Khodagholy, J. N. Gelinas, T. Thesen, W. Doyle, O. Devinsky, G. G. Malliaras, G. Buzsáki, *Nat. Neurosci.* **2014**, *18*, 310–315.

[4] a) P. J. Molino, G. G. Wallace, *Appl. Phys. Lett. Mater.* **2015**, *3*, 014913; b) A. Chortos, Z. Bao, *Mater. Today* **2014**, *17*, 321–331; c) M. Drack, I. Graz, T. Sekitani, T. Someya, M. Kaltenbrunner, S. Bauer, *Adv. Mater.* **2015**, *27*, 34–40.

[5] K. Svennersten, K. C. Larsson, M. Berggren, A. Richter-Dahlfors, *Biochim. Biophys. Acta Gen. Subj.* **2011**, *1810*, 276–285.

[6] M. Y. Mulla, E. Tuccori, M. Magliulo, G. Lattanzi, G. Palazzo, K. Persaud, L. Torsi, *Nat. Commun.* **2015**, *6*, 6010.

[7] a) S. H. Kim, K. Hong, W. Xie, K. H. Lee, S. Zhang, T. P. Lodge, C. D. Frisbie, *Adv. Mater.* **2013**, *25*, 1822–1846; b) L. Torsi, M. Magliulo, K. Manoli, G. Palazzo, *Chem. Soc. Rev.* **2013**, *42*, 8612–8628.

[8] a) M. Irimia-Vladu, *Chem. Soc. Rev.* **2014**, *43*, 588–610; b) A. Campana, T. Cramer, D. T. Simon, M. Berggren, F. Biscarini, *Adv. Mater.* **2014**, *26*, 3874–3878.

[9] F. Werkmeister, B. Nickel, *J. Mater. Chem. B* **2013**, *1*, 3830–3835.

[10] a) D. Töbjork, R. Österbacka, *Adv. Mater.* **2011**, *23*, 1935–1961; b) P. J. Wojcik, L. Santos, L. Pereira, R. Martins, E. Fortunato, *Nanoscale* **2015**, *7*, 1696–1708; c) S. Thiemann, S. J. Sachnov, F. Pettersson, R. Bollström, R. Österbacka, P. Wasserscheid, J. Zaumseil, *Adv. Funct. Mater.* **2014**, *24*, 625–634.

[11] C. P. Tan, B. R. Cipriany, D. M. Lin, H. G. Craighead, *Nano Lett.* **2010**, *10*, 719–725.

[12] http://www.researchandmarkets.com/reports/2090646/.

[13] E. Fortunato, P. Barquinha, R. Martins, *Adv. Mater.* **2012**, *24*, 2945–2986.

[14] a) K. Balasubramanian, K. Kern, *Adv. Mater.* **2014**, *26*, 1154–1175; b) S. Liu, X. Guo, *NPG Asia Mater.* **2012**, *4*, e23; c) M. D. Angione, R. Pilolli, S. Cotrone, M. Magliulo, A. Mallardi, G. Palazzo, L. Sabbatini, D. Fine, A. Dodabalapur, N. Cioffi, L. Torsi, *Mater. Today* **2011**, *14*, 424–433.

[15] F. Chen, Q. Qing, J. Xia, N. Tao, *Chem. Asian J.* **2010**, *5*, 2144–2153.

[16] D. T. Simon, S. Kurup, K. C. Larsson, R. Hori, K. Tybrandt, M. Goiny, E. W. Jager, M. Berggren, B. Canlon, A. Richter-Dahlfors, *Nat. Mater.* **2009**, *8*, 742–746.

[17] P. Leleux, J. Rivnay, T. Lonjaret, J. M. Badier, C. Bénar, T. Hervé, P. Chauvel, G. G. Malliaras, *Adv. Healthcare Mater.* **2015**, *4*, 142–147.

[18] S. A. Tria, M. Ramuz, M. Huerta, P. Leleux, J. Rivnay, L. H. Jimison, A. Hama, G. G. Malliaras, R. M. Owens, *Adv. Healthcare Mater.* **2014**, *3*, 1053–1060.

[19] C. R. Kagan, P. Andry, *Thin-film transistors* (Eds.: C. R. Kagan, P. Andry), Marcel Dekker, New York, **2003**.

[20] S. M. Sze, K. K. Ng, *Physics of semiconductor devices*, 3rd ed., Wiley, Hoboken, **2006**.

[21] a) R. M. Owens, G. G. Malliaras, *MRS Bull.* **2010**, *35*, 449–456; b) G. Tarabella, G. Nanda, M. Villani, N. Coppedè, R. Mosca, G. G. Malliaras, C. Santato, S. Iannotta, F. Cicoira, *Chem. Sci.* **2012**, *3*, 3432–3435.

[22] a) L. Kergoat, B. Piro, M. Berggren, G. Horowitz, M.-C. Pham, *Anal. Bioanal. Chem.* **2012**, *402*, 1813–1826; b) C. Liao, M. Zhang, M. Y. Yao, T. Hua, L. Li, F. Yan, *Adv. Mater.* **2015**, *27*, 676–681; c) R. Porrazzo, S. Bellani, A. Luzio, C. Bertarelli, G. Lanzani, M. Caironi, M. Antognazza, *Appl. Phys. Lett. Mater.* **2015**, *3*, 0149051–0149058.

[23] a) M. Demelas, S. Lai, A. Spanu, S. Martinoia, P. Cosseddu, M. Barbaro, A. Bonfiglio, *J. Mater. Chem. B* **2013**, *1*, 3811–3819; b) T. Minamiki, T. Minami, R. Kurita, O. Niwa, S.-i. Wakida, K. Fukuda, D. Kumaki, S. Tokito, *Appl. Phys. Lett.* **2014**, *104*, 243703; c) M. Kamahori, Y. Ishige, M. Shimoda, *Biosens. Bioelectron.* **2008**, *23*, 1046–1054.

[24] a) O. Knopfmacher, M. L. Hammock, A. L. Appleton, G. Schwartz, J. Mei, T. Lei, J. Pei, Z. Bao, *Nat. Commun.* **2014**, *5*, 2954; b) M. Magliulo, K. Manoli, E. Macchia, G. Palazzo, L. Torsi, *Adv. Mater.* **2014**, DOI: 10.1002/adma.201403477; c) V. Benfenati, S. Toffanin, S. Bonetti, G. Turatti, A. Pistone, M. Chiappalone, A. Sagnella, A. Stefani, G. Generali, G. Ruani, D. Saguatti, R. Zamboni, M. Muccini, *Nat. Mater.* **2013**, *12*, 672–680.

[25] M. J. Spijkman, J. J. Brondijk, T. C. Geuns, E. C. Smits, T. Cramer, F. Zerbetto, P. Stoliar, F. Biscarini, P. W. Blom, D. M. de Leeuw, *Adv. Funct. Mater.* **2010**, *20*, 898–905.

[26] M. L. Hammock, O. Knopfmacher, B. D. Naab, J. B.-H. Tok, Z. Bao, *ACS Nano* **2013**, *7*, 3970–3980.

[27] a) M. D. Angione, S. Cotrone, M. Magliulo, A. Mallardi, D. Altamura, C. Giannini, N. Cioffi, L. Sabbatini, E. Fratini, P. Baglioni, G. Scamarcioe, G. Palazzo, L. Torsi, *Proc. Natl. Acad. Sci. USA* **2012**, *109*, 6429–6434; b) M. Magliulo, A. Mallardi, R. Gristina, F. Ridi, L. Sabbatini, N. Cioffi, G. Palazzo, L. Torsi, *Anal. Chem.* **2013**, *85*, 3849–3857.

[28] B. Crone, A. Dodabalapur, A. Gelperin, L. Torsi, H. Katz, A. Lovinger, Z. Bao, *Appl. Phys. Lett.* **2001**, *78*, 2229–2231.

[29] M. E. Roberts, S. C. Mannsfeld, N. Queraltó, C. Reese, J. Locklin, W. Knoll, Z. Bao, *Proc. Natl. Acad. Sci. USA* **2008**, *105*, 12134–12139.

[30] P. Bergveld, *Sens. Actuators B* **2003**, *88*, 1 – 20.
[31] A. Spanu, S. Lai, P. Cosseddu, M. Tedesco, S. Martinoia, A. Bonfiglio, *Sci. Rep.* **2015**, *5*, 8807.
[32] X. Strakosas, M. Bongo, R. M. Owens, *J. Appl. Polym. Sci.* **2015**, *132*, 41735 – 41735.
[33] D. Khodagholy, T. Doublet, P. Quilichini, M. Gurfinkel, P. Leleux, A. Ghestem, E. Ismailova, T. Hervé, S. Sanaur, C. Bernard, G. G. Malliaras, *Nat. Commun.* **2013**, *4*, 1 – 7.
[34] a) H. E. Katz, *Electroanalysis* **2004**, *16*, 1837 – 1842; b) D. Duarte, A. Dodabalapur, *J. Appl. Phys.* **2012**, *111*, 0445091 – 0445097.
[35] T. Cramer, A. Campana, F. Leonardi, S. Casalini, A. Kyndiah, M. Murgia, F. Biscarini, *J. Mater. Chem. B* **2013**, *1*, 3728 – 3741.
[36] R. DiCosimo, J. McAuliffe, A. J. Poulose, G. Bohlmann, *Chem. Soc. Rev.* **2013**, *42*, 6437 – 6474.
[37] N. Durán, M. A. Rosa, A. D'Annibale, L. Gianfreda, *Enzyme Microb. Technol.* **2002**, *31*, 907 – 931.
[38] S. Federici, G. Oliviero, K. Hamad-Schifferli, P. Bergese, *Nanoscale* **2010**, *2*, 2570 – 2574.
[39] a) R. Grange, J. Thompson, D. Lambert, *Br. J. Anaesth.* **2014**, *112*, 213 – 216; b) S. D. Gan, K. R. Patel, *J. Invest. Dermatol.* **2013**, *133*, e12; c) J. Hu, S. Wang, L. Wang, F. Li, B. Pingguan-Murphy, T. J. Lu, F. Xu, *Biosens. Bioelectron.* **2014**, *54*, 585 – 597.
[40] J. Homola, *Chem. Rev.* **2008**, *108*, 462 – 493.
[41] H.-F. Ji, H. Gao, K. R. Buchapudi, X. Yang, X. Xu, M. K. Schulte, *Analyst* **2008**, *133*, 434 – 443.
[42] D. Maiolo, S. Federici, L. Ravelli, L. E. Depero, K. Hamad-Schifferli, P. Bergese, *J. Colloid Interface Sci.* **2013**, *402*, 334 – 339.
[43] a) P. Jonkheijm, D. Weinrich, H. Schröder, C. M. Niemeyer, H. Waldmann, *Angew. Chem. Int. Ed.* **2008**, *47*, 9618 – 9647; *Angew. Chem.* **2008**, *120*, 9762 – 9792; b) F. Rusmini, Z. Zhong, J. Feijen, *Biomacromolecules* **2007**, *8*, 1775 – 1789.
[44] M. Rabe, D. Verdes, S. Seeger, *Adv. Colloid Interface Sci.* **2011**, *162*, 87 – 106.
[45] a) P. Stoliar, E. Bystrenova, S. Quiroga, P. Annibale, M. Facchini, M. Spijkman, S. Setayesh, D. De Leeuw, F. Biscarini, *Biosens. Bioelectron.* **2009**, *24*, 2935 – 2938; b) P. Lin, F. Yan, *Adv. Mater.* **2012**, *24*, 34 – 51.
[46] L. S. Wong, F. Khan, J. Micklefield, *Chem. Rev.* **2009**, *109*, 4025 – 4053.
[47] a) R. G. Nuzzo, D. L. Allara, *J. Am. Chem. Soc.* **1983**, *105*, 4481 – 4483; b) Z. Matharu, A. J. Bandodkar, V. Gupta, B. D. Malhotra, *Chem. Soc. Rev.* **2012**, *41*, 1363 – 1402; c) N. K. Chaki, K. Vijayamohanan, *Biosens. Bioelectron.* **2002**, *17*, 1 – 12; d) C. D. Bain, E. B. Troughton, Y. T. Tao, J. Evall, G. M. Whitesides, R. G. Nuzzo, *J. Am. Chem. Soc.* **1989**, *111*, 321 – 335.
[48] a) H. U. Khan, M. E. Roberts, O. Johnson, R. Förch, W. Knoll, Z. Bao, *Adv. Mater.* **2010**, *22*, 4452 – 4456; b) M. Magliulo, A. Mallardi, M. Y. Mulla, S. Cotrone, B. R. Pistillo, P. Favia, I. Vikholm-Lundin, G. Palazzo, L. Torsi, *Adv. Mater.* **2013**, *25*, 2090 – 2094.
[49] M. Magliulo, B. R. Pistillo, M. Y. Mulla, S. Cotrone, N. Ditaranto, N. Cioffi, P. Favia, L. Torsi, *Plasma Processes Polym.* **2013**, *10*, 102 – 109.
[50] L. Kergoat, B. Piro, M. Berggren, M.-C. Pham, A. Yassar, G. Horowitz, *Org. Electron.* **2012**, *13*, 1 – 6.
[51] L. Kergoat, B. Piro, D. T. Simon, M. C. Pham, V. Noël, M. Berggren, *Adv. Mater.* **2014**, *26*, 5658 – 5664.
[52] J. Turková, *J. Chromatogr. B* **1999**, *722*, 11 – 31.
[53] G. Palazzo, D. De Tullio, M. Magliulo, A. Mallardi, F. Intranuovo, M. Y. Mulla, P. Favia, I. Vikholm-Lundin, L. Torsi, *Adv. Mater.* **2015**, *27*, 911-916.
[54] C. Suspène, B. Piro, S. Reisberg, M.-C. Pham, H. Toss, M. Berggren, A. Yassar, G. Horowitz, *J. Mater. Chem. B* **2013**, *1*, 2090 – 2097.
[55] I. Vikholm-Lundin, S. Auer, M. Paakkunainen, J. A. Määttä, T. Munter, J. Leppiniemi, V. P. Hytönen, K. Tappura, *Sens. Actuators B* **2012**, *171*, 440 – 448.
[56] A. W. Adamson, A. P. Gast, *Physical chemistry of surfaces*, 6th ed., Wiley, New York, **1997**.
[57] R. Sips, *J. Chem. Phys.* **1948**, *16*, 490 – 495.
[58] J. N. Weiss, *FASEB J.* **1997**, *11*, 835 – 841.
[59] a) Y. Liu, Y.-J. Liu, *Sep. Purif. Technol.* **2008**, *61*, 229 – 242; b) S. Cazalbou, G. Bertrand, C. Drouet, *J. Phys. Chem. B* **2015**, *119*, 3014 – 3024.
[60] A. Liscio, V. Palermo, P. Samori, *Acc. Chem. Res.* **2010**, *43*, 541 – 550.
[61] R. Levicky, A. Horgan, *Trends Biotechnol.* **2005**, *23*, 143 – 149.
[62] G. Oliviero, S. Federici, P. Colombi, P. Bergese, *J. Mol. Recognit.* **2011**, *24*, 182 – 187.
[63] W. Brattain, C. Garrett, *Publs. Monograph* **1955**, *2372*, 1.
[64] a) M. J. Panzer, C. R. Newman, C. D. Frisbie, *Appl. Phys. Lett.* **2005**, *86*, 103503; b) L. Kergoat, L. Herlogsson, D. Braga, B. Piro, M. C. Pham, X. Crispin, M. Berggren, G. Horowitz, *Adv. Mater.* **2010**, *22*, 2565 – 2569.
[65] A. Al Naim, M. Grell, *Appl. Phys. Lett.* **2012**, *101*, 141603.
[66] T. Cramer, A. Kyndiah, M. Murgia, F. Leonardi, S. Casalini, F. Biscarini, *Appl. Phys. Lett.* **2012**, *100*, 143302.
[67] M. J. Panzer, C. D. Frisbie, *Adv. Funct. Mater.* **2006**, *16*, 1051 – 1056.
[68] a) A. Dodabalapur, L. Torsi, H. Katz, *Science* **1995**, *268*, 270 – 271; b) A. Laiho, L. Herlogsson, R. Forchheimer, X. Crispin, M. Berggren, *Proc. Natl. Acad. Sci. USA* **2011**, *108*, 15069 – 15073.
[69] P. Kukic, D. Farrell, L. P. McIntosh, B. García-Moreno, E. K. S. Jensen, Z. Toleikis, K. Teilum, J. E. Nielsen, *J. Am. Chem. Soc.* **2013**, *135*, 16968 – 16976.
[70] F. Buth, D. Kumar, M. Stutzmann, J. Garrido, *Appl. Phys. Lett.* **2011**, *98*, 153302 – 153303.
[71] K. Manoli, M. M. Patrikoussakis, M. Magliulo, L. M. Dumitru, M. Y. Mulla, L. Sabbatini, L. Torsi, *Org. Electron.* **2014**, *15*, 2372 – 2380.
[72] S. J. Park, O. S. Kwon, S. H. Lee, H. S. Song, T. H. Park, J. Jang, *Nano Lett.* **2012**, *12*, 5082 – 5090.
[73] a) T. H. Kim, S. H. Lee, J. Lee, H. S. Song, E. H. Oh, T. H. Park, S. Hong, *Adv. Mater.* **2009**, *21*, 91 – 94; b) H. Yoon, S. H. Lee, O. S. Kwon, H. S. Song, E. H. Oh, T. H. Park, J. Jang, *Angew. Chem. Int. Ed.* **2009**, *48*, 2755 – 2758; *Angew. Chem.* **2009**, *121*, 2793 – 2796.
[74] S. Casalini, F. Leonardi, T. Cramer, F. Biscarini, *Org. Electron.* **2013**, *14*, 156 – 163.
[75] H. Tang, P. Lin, H. L. Chan, F. Yan, *Biosens. Bioelectron.* **2011**, *26*, 4559 – 4563.
[76] M. Zhang, C. Liao, Y. Yao, Z. Liu, F. Gong, F. Yan, *Adv. Funct. Mater.* **2014**, *24*, 978 – 985.

Received: March 21, 2015
Published online: September 30, 2015